Indole substituted zinc phthalocyanine: Improved photosensitizing ability and modified photooxidation mechanism

ARTICLE *in* JOURNAL OF PHOTOCHEMISTRY AND PHOTOBIOLOGY A: CHEMISTRY · DECEMBER 2011

Impact Factor: 2.5 · DOI: 10.1016/j.jphotochem.2011.10.008

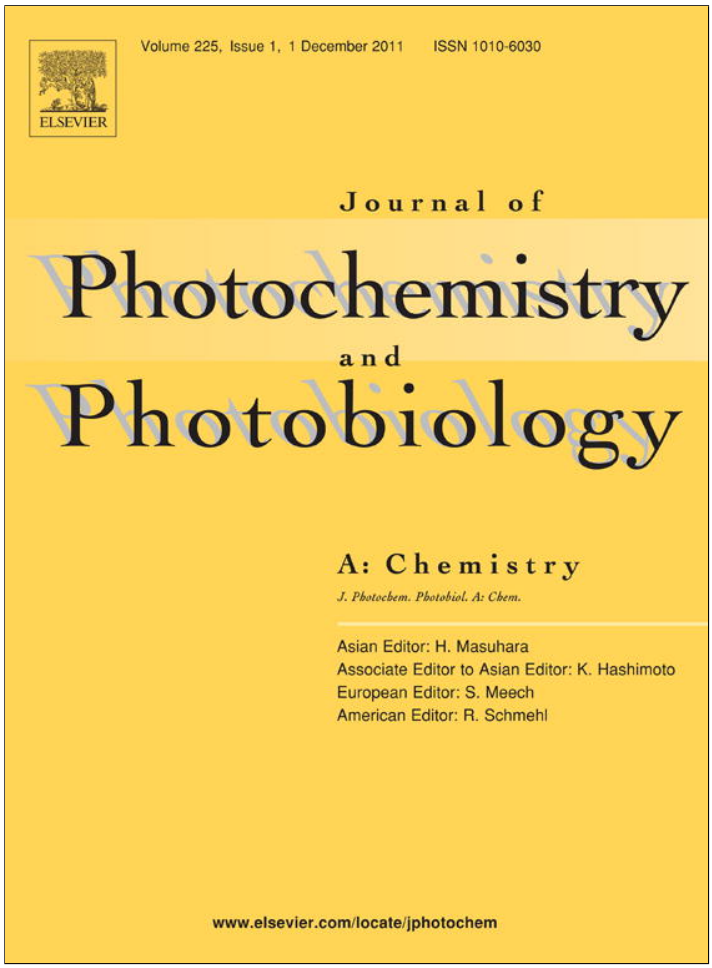

Journal of Photochemistry and Photobiology A: Chemistry 225 (2011) 117–124

Contents lists available at SciVerse ScienceDirect

Journal of Photochemistry and Photobiology A: Chemistry

journal homepage: www.elsevier.com/locate/jphotochem

Indole substituted zinc phthalocyanine: Improved photosensitizing ability and modified photooxidation mechanism

Xian-Fu Zhang[a,b,*], Wenfeng Guo[a]

[a] Chemistry Department & Center of Instrumental Analysis, Hebei Normal University of Science and Technology, Qinghuangdao, Hebei Province 066004, China
[b] MPC Technologies, Hamilton, Ontario, Canada L8S 3H4

ARTICLE INFO

Article history:
Received 8 June 2011
Received in revised form
16 September 2011
Accepted 3 October 2011
Available online 10 October 2011

Keywords:
Phthalocyanine
Indole
Photosensitizer
Photophysics
Singlet oxygen
Fluorescence
Electron transfer

ABSTRACT

The photophysical and photochemical processes within a novel photosensitizer (PS), zinc phthalocyanine (ZnPc) modified by indole units, were explored. The properties related to photodynamic therapy of tumor (PDT) were studied by time-resolved transient UV–vis absorption spectra, steady state and time-resolved fluorescence spectra, and chemical trapping of singlet oxygen by diphenylisobenzofuran (DPBF). Intramolecular photoinduced electron transfer (PET) within the conjugate from the indole subunits (donor A), to S_1 (excited singlet state) of ZnPc moiety (acceptor D), is featured by the significant decrease of fluorescence quantum yield and lifetime of ZnPc moiety, and the occurrence of transient absorption bands of $ZnPc^{\bullet-}$ at 570 and 630 nm. The triplet state, on the other hand, was not quenched by indole units. The kinetics and thermodynamics of PET were analyzed quantitatively, and the quantum efficiency of PET is computed to be 38%, almost double of the emission efficiency (20%). The quantum efficiency of triplet (T_1) formation is 0.50 and the quantum yield of DPBF photooxidation is 0.72. Both are larger than the expected value of 0.32. The evolution of transient absorption spectra showed that the charge separation state ($ZnPc^{\bullet-}$–$indole^{\bullet+}$) recombined to triplet state ZnPc(T_1)–indole, which is responsible for the high yield of T_1 formation. In the presence of oxygen, both T_1 and $ZnPc^{\bullet-}$ were quenched efficiently, which forms singlet oxygen and superoxide anion, respectively. DPBF is therefore photo-oxidized by both singlet oxygen (Type II reaction, 46%) and superoxide anion radical (Type I reaction, 54%), which led to the high yield of photooxidation. This is in contrast to free ZnPc PS, in which only singlet oxygen is responsible for the photooxidation. The result suggests that the reaction mechanism is changed upon conjugation so that the importance of Type I reaction is greatly enhanced, and the indole-conjugated ZnPc is an even better PS than the free ZnPc.

1. Introduction

Photodynamic therapy of tumor (PDT) is under intensively developing to address the lack of selectivity in removing and destroying tumor tissues by traditional cancer therapies, such as surgery, radiotherapy, and chemotherapy [1–3]. The interaction of a photosensitizer (PS) with biomolecules in the presence of light plays the key role to understand the mechanism for PDT and design the new generation drugs for it [3]. There have been a lot of mechanism studies in which aqueous solution was used as the medium and amino acids were employed as substrates for photosensitized electron transfer or singlet oxygen quenching [4–9]. Intermolecular interactions in aqueous solution between a PS and amino acids are probably quite different from that in the solid tumor tissue. The localization of PS within tumor tissues brings various aromatic electron donor moieties, such as N-containing amino acid residues, into its much closer vicinity than that in aqueous solution, hence the interaction is more similar to that of intramolecular electron donor–acceptor case (interaction through bonding). The intermolecular photoinduced electron transfer (PET) between free phthalocyanine PS and amino acid donors has been evidenced previously [4–9]. The PS functionalized by biomolecules can be considered as intra-molecular electron donor–acceptor pairs, which usually make PET or energy transfer process from S_1 (lowest excited singlet state) of PS much faster than that of intermolecular cases. PET competes with intersystem crossing (ISC) and therefore reduces the efficiency of triplet formation, which further decreases the yield of singlet oxygen and its subsequent photooxidation (Type II reaction). PET also forms charge separated state (CSS) radical pairs that can reduce oxygen to superoxide anion radicals, both CSS and $O_2^{\bullet-}$ may also participate photooxidations of biological substrates, and hence enhances Type I reaction. It is therefore helpful

* Corresponding author at: Chemistry Department & Center of Instrumental Analysis, Hebei Normal University of Science and Technology, Qinghuangdao, Hebei Province 066004, China. Tel.: +86 3358357040; fax: +86 3358357040.
E-mail address: zhangxianfu@tsinghua.org.cn (X.-F. Zhang).

1010-6030/$ – see front matter © 2011 Elsevier B.V. All rights reserved.
doi:10.1016/j.jphotochem.2011.10.008

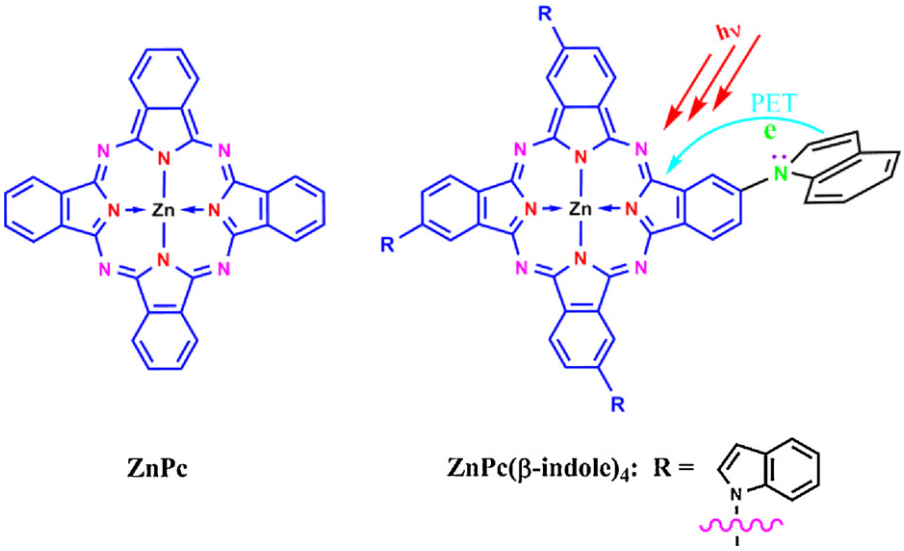

Fig. 1. Chemical Structure of ZnPc(β-indole)$_4$.

to evaluate how the bioconjugation of PS affects the photosensitizing process of PDT, whereas the past focus of related investigations has been placed on the synthesis of PS bioconjugates and their biological activities. Proteins or peptides contain up to twenty three amino acid residues, all of these could act as electron donors which make the clear elucidation of photo events within protein/peptide conjugated PS difficult. Tryptopan and tyrosine, however, are generally considered as the most active components in protein for PDT. To simplify the problem, indole, the main reactive component in tryptophan, was selected and attached to zinc phthalocyanine (ZnPc) in this study (Fig. 1). ZnPc was selected since its derivatives have been tested both in vitro [7,10–19] and in vivo [20,21] to be effective photosensitizers for PDT. We show in this report that the indole-modification of ZnPc significantly changes the mechanism of photosensitized oxidation while improves the photosensitizing ability.

2. Experimental

2.1. Reagents and apparatus

All reagents for synthesis were analytical grade and used as received. Dimethylformide (DMF) was dried and redistilled before use. ^{1}H NMR spectra were recorded at room temperature on a Bruker dmx 300 MHz NMR spectrometer. MS spectra were recorded either on a Bruker APEX II or Autoflex III Maldi-TOF spectrometer. IR spectra were recorded at room temperature on a Shimadzu FTIR-8900 spectrometer. UV–vis spectra were recorded on a Shimadzu 4500 spectrophotometer using 1 cm matched quartz cuvettes.

2.2. Synthesis

2.2.1. Synthesis of 4-(indol-1-yl)phthalonitrile

1.73 g (0.01 mol) 4-nitrophthalonitrile and 1.17 g (0.01 mol) indole were added to 20 ml DMF in argon atmosphere, the resulted solution was stirred at room temperature under argon for 48 h, during which 4.1 g (0.03 mol) anhydrous potassium carbonate was added in four equal portions every 2 h. The product solution was then poured into 100 ml ice-water to precipitate, the filtered solid was washed with water neutral pH and dried under vacuum. Slightly yellow solid was obtained after recrystallization with hexane–methanol solvent. Yield: 43%. m.p. 142–143 °C. IR(KBr), ν(cm^{-1}): 3027, 1597, 1456 (Ar–H), 2233 (C≡N), 1070 (Ar–N). ^{1}H NMR ($CDCl_3$, ppm): δ 8.05–8.09 (d, 1H), 7. 97 (s, 1H), 7.88–7.95 (m, 2H), 7.70–7.72 (d, 1H), 7.63–7.66 (d, 1H), 7.33–7.35 (m, 2H), 6.81–6.82 (d, 1H). MS, *m*/*z*: 243 [M$^+$].

2.2.2. Synthesis of tetra[β-(indol-1-yl)] ZnPc, ZnPc(β-indole)$_4$

The two-step procedure for the synthesis of ZnPc(β-indole)$_4$ is shown in Fig. 2. It is a well established procedure which has been extensively discussed in literature [27].

Zinc acetate (0.070 g, 0.33 mmol), 4-(indol-1-yl)phthalonitrile (0.31 g, 1.3 mmol), and 8 ml dried *n*-pentanol were mixed and stirred at 135 °C for 4 h under argon atmosphere in the presence of two drops of DBU as catalyst. After cooling down, the green precipitate was collected by filtration and washed with *n*-pentanol and *n*-hexane. The dried crude product was dissolved in CH_2Cl_2 and purified by column chromatography (silica gel) using CH_2Cl_2 as the mobile phase. Yield: 39%. UV–vis (DMF): λ_{max} nm (log ε) 366 (4.66), 620 (4.41), 686 (5.10). IR [(KBr) ν_{max}/cm^{-1}]: 3053 (Ar–H), 1608, 1519, 1490, 1332, 1137, 1049, 742 (Pc ring C=C etc.), 895(N–Zn). ^{1}H NMR ($CDCl_3$): δ, ppm 9.10–9.16 (4H, m), 8.88–8.91 (4H, m), 7.89–8.31 (16H, m), 7.27–7.55 (8H, m), 6.97–7.05 (4H, d). Anal. ($C_{64}H_{36}N_{12}Zn$): C, H, N. MALDI-TOF-MS *m*/*z*: calculated 1036.3; found 1037.6 (M+1).

2.3. Photophysical measurements

The absorption and fluorescence spectra, fluorescence quantum yields and excited singlet-state lifetimes, as well as triplet properties were investigated at room temperature ca 22 °C. Steady-state fluorescence spectra were acquired on a FLS 920 instrument. All spectra were corrected for the sensitivity of the photo-multiplier tube. The fluorescence quantum yield (Φ_f) was measured by using

$$\Phi_f = \Phi_f^0 \cdot \frac{F_s}{F_0} \cdot \frac{A_0}{A_s} \frac{n_s^2}{n_0^2}$$

in which *F* is the integrated fluorescence intensity, *A* is the absorbance at excitation wavelength, *n* is the refractive index of the solvent used, the subscript 0 stands for a reference compound and s represents samples. ZnPc was used as the reference ($\Phi_f^0 = 0.30$) [22,23]. Excitation wavelengths of 610 nm corresponding to the vibronic band of S_0 to S_1 transitions were employed. The sample and reference solutions were prepared with the same absorbance

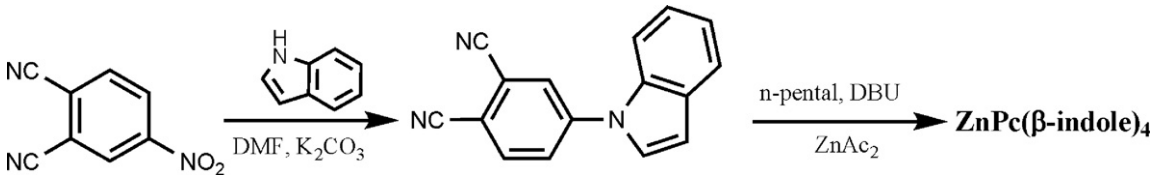

Fig. 2. Synthetic path for ZnPc(β-indole)$_4$.

(A_i) at the excitation wavelength (near 0.09) in the same solvent DMF. All solutions were air saturated for Φ_f measurements.

Fluorescence lifetime of S_1 was measured by time-correlated single photon counting method (Edinburgh FLS920 spectrophotometer) with excitation at 672 nm diode laser (50 ps FWHM) and emission was monitored at 690 nm and 730 nm.

Transient absorption spectra were recorded in degassed DMF (prepared by bubbling with argon for 20 min) with an Edinburgh LP920 laser flash photolysis system. A Nd:YAG laser (Brio, 355 nm and 4 ns FWHM) was used as excitation source. The analyzing light was from a pulsed xenon lamp. The laser and analyzing light beams perpendicularly passed through a quartz cell with an optical path length of 1 cm. The signal was displayed and recorded on a Tektronix TDS 3012B oscilloscope and an R928B detector. The laser energy incident at the sample was attenuated to ca. 20 mJ per pulse. Time profiles at a series of wavelengths from which point by-point spectra were assembled were recorded with the aid of a Pc controlled kinetic absorption spectrometer. The concentrations of the target compounds were typically 15 μM providing A_{355} = 0.40 in a 10 mm cuvette.

The triplet–triplet absorption coefficients ($\Delta\varepsilon_T$) of the samples were obtained using the singlet depletion method [24], and the following equation was used to calculate the $\Delta\varepsilon_T$:

$$\Delta\varepsilon_T = \varepsilon_S \frac{\Delta A_T}{\Delta A_S} \quad (1)$$

where ΔA_S and ΔA_T are the absorbance change of the triplet transient difference absorption spectrum at the minimum of the bleaching band and the maximum of the positive band, respectively, and ε_S is the ground-state molar absorption coefficient at the UV–vis absorption band maximum. Both ΔA_S and ΔA_T were obtained from the triplet transient difference absorption spectra.

The triplet quantum yield Φ_T was obtained by comparing the ΔA_T of the optically matched sample solution at 355 nm in a 1 cm cuvette to that of the reference using the equation [24]:

$$\Phi_T = \Phi_T^{ZnPc} \cdot \frac{\Delta A_T}{\Delta A_T^{ZnPc}} \cdot \frac{\Delta\varepsilon_T^{ZnPc}}{\Delta\varepsilon_T}, \quad (2)$$

where the superscript represents the reference, ΔA_T is the absorbance of the triplet transient difference absorption spectrum at the selected wavelength, and $\Delta\varepsilon_T$ is the triplet state molar absorption coefficient.

Singlet oxygen quantum yield (Φ_Δ) determinations were carried out using the chemical trapping method [25]. Typically, a 3 ml portion of the respective PS solutions that contained diphenylisobenzofuran (DPBF) was irradiated at 660 nm in air saturated DMF. Φ_Δ value was obtained by the relative method using ZnPc as the reference (Eq. (3)):

$$\Phi_\Delta = \Phi_\Delta^{ref} \frac{k}{k^{ref}} \frac{I_a^{ref}}{I_a}, \quad (3)$$

where Φ_Δ^{ref} is the singlet oxygen quantum yield for the standard (0.60 for ZnPc in DMF) [26], k and k^{ref} are the DPBF photo-bleaching rate constants in the presence of the respective samples and standard, respectively; I_a and I_a^{ref} are the rates of light absorption at the irradiation wavelength of 660 nm by the samples and standard, respectively. Their ratio can be obtained by Eq. (4).

$$\frac{I_a^{ref}}{I_a} = \frac{1 - 10^{-A_{670}^{ref}}}{1 - 10^{-A_{670}}}. \quad (4)$$

To avoid chain reactions induced by DPBF in the presence of singlet oxygen, the concentration of DPBF was lowered to ~3×10^{-5} mol dm^{-3}. A solution of sensitizer (absorbance ~0.70 at the irradiation wavelength) that contained DPBF was prepared in the dark and irradiated in the Q-band region. DPBF degradation was monitored by UV–vis absorption spectrum. The error in the determination of Φ_Δ was ~10% (determined from several Φ_Δ values).

3. Results and discussion

The main concern of this study is how the conjugated indole moieties affect the behavior of the excited state of ZnPc, including S_1 (lowest excited singlet state) and T_1 (lowest excited triplet state), and its capability as PS. All the related data is collected in Table 1, together with that of the unconjugated ZnPc for comparison. The S_1 properties of the conjugate were revealed by absorption (Fig. 3) and fluorescence measurements, including the spectral data, the fluorescence quantum yield (Φ_f), and fluorescence lifetime (τ_f). Φ_f of ZnPc(β-indole)$_4$ is decreased one-third compared to that of ZnPc. The τ_f of the major emitting component is also shortened to one-third, matching the Φ_f decrease. This fluorescence quenching shows that the indole conjugation significantly affects the behavior of S_1 of ZnPc, and that the interaction between S_1 of ZnPc and indole units does occur, which may be photoinduced electron transfer (PET), or energy transfer (PeT), etc.

To understand the above observation, measurements on absorption spectra for T_1 and other transient species were carried out. Studies on μs transient absorption spectra (TAS) in Fig. 4 gave the T_1 properties (Table 1), while nano second TAS (Fig. 5) led to the identification of ZnPc$^{\bullet-}$ formed by PET from indole units (donor D) to

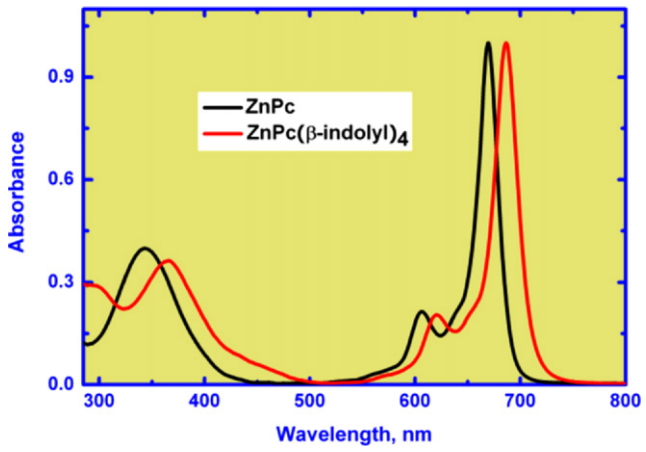

Fig. 3. Comparison of the UV–vis absorption spectrum of ZnPc (4 μM) with that of ZnPc(β-indole)$_4$ (7.9 μM) in DMF.

Table 1
Photophysical properties in DMF.[a]

	λ_{max}^{abs} (nm)	log ε	λ_{max}^{em} (nm)	$\Delta\bar{\nu}$ (cm^{-1})	E_s (eV)	Φ_f	τ_f (ns)	χ^2	λ_{max}^{T-T} (nm)	$\Delta\varepsilon_T$ (M^{-1}cm^{-1})	Φ_T	τ_T (μs)	Φ_Δ	Φ_{PET}
ZnPc	668	5.40	680	264.2	1.85	0.30	3.60	1.19	470	35,620	0.60	113	0.60	n.a.
ZnPc(β–indole)$_4$	686	5.10	697	230.1	1.83	0.20	2.22(87%), 4.91(13%)	1.11	520	31,715	0.50	107	0.72	0.38

[a] λ_{max}^{abs} is the UV–vis absorption maximum. λ_{max}^{em} is the fluorescence emission maximum. $\Delta\bar{\nu}$ is the Stoke's shift. E_s is the energy of lowest excited state (S_1). Φ_f is the fluorescence quantum yield, τ_f is the fluorescence lifetime. χ^2 is the Chi squared value for the fitting of emission decay.

S_1 state of ZnPc moiety (acceptor A): D–A$\xrightarrow{h\nu}$D–A(S_1) → D$^{\bullet+}$–A$^{\bullet-}$. The details will be discussed in later sections.

3.1. Ground state absorption

Fig. 3 compares the UV–vis absorption spectrum of ZnPc with that of ZnPc(β-indole)$_4$. In red region, the spectral shape of the two spectra is almost identical, indicating that the geometry of the π skeleton of ZnPc moiety within ZnPc(β-indole)$_4$ is the same as that of free ZnPc. In other words, it is not altered by the linked indoles. Upon the attachment of four indole units, the absorption maximum (λ_{max}^{abs}) is only red shifted by 18 nm. This small shift suggests that the indole aromatic system is not π-conjugated with the ZnPc aromatic ring, even though the indole's nitrogen atom is directly connected to ZnPc. The molecular dynamic calculation by MM2 suggests that the dihedral angle is around 30° between the two types of aromatic rings in the ground state.

Due to the mutual independence of the two types of aromatic system, an indole sub-unit behaves just like an usual electron-donating group with respect to λ_{max}^{abs} of ZnPc. In the UV region of the spectrum for ZnPc(β-indole)$_4$, a band around 280 nm due to indole chromophore appears, which is another evidence that indoles are indeed linked to ZnPc.

3.2. μs scaled transient absorption spectra

Fig. 4 displays the μs-scale transient absorption spectra (TAS) for ZnPc(β-indole)$_4$ and ZnPc. These spectra were recorded in argon saturated DMF with excitation at 355 nm by a 4 *ns* pulsed laser. TAS of ZnPc (Fig. 4b) is the typical of triplet–triplet (T_1–T_n) absorptions for Pcs and in good agreement with that reported for ZnPc [24]. TAS of ZnPc(β-indole)$_4$ (Fig. 4a) exhibits very similar spectral shape to that of ZnPc, except for a red shift of the absorption maximum, which is then assigned to T_1 of ZnPc(β-indole)$_4$ by analogy and also based on the following analysis.

The minimum of negative absorptions in the B- and Q-band region showed peaks matching the absorption maximum of the corresponding ground state absorption; the positive bands are separated from the ground state bleaching with well defined isosbestic points, and the bleaching recovery are synchronous to the

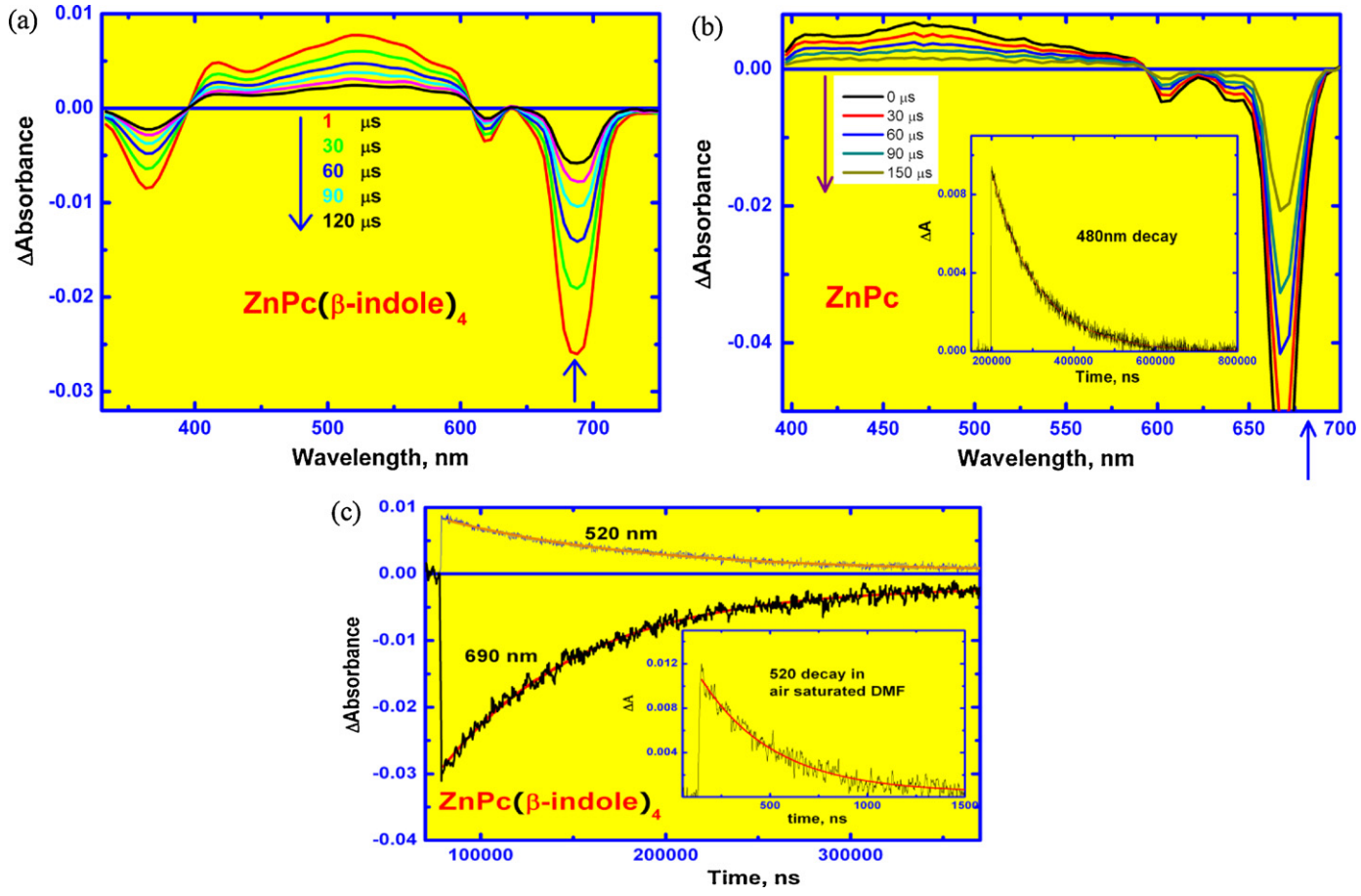

Fig. 4. μs scaled transient absorption spectra of ZnPc(β-indole)$_4$ (a) and ZnPc (b) in argon purged DMF, 15 μM, excitation wavelength 355 nm. Inset of ZnPc shows the decay at 480 nm. (c) Decay of positive transient signal and recovery of negative ground state absorption in argon saturated DMF for ZnPc(β-indole)$_4$, excitation with 355 nm laser pulse. Inset is the decay at 520 nm in air saturated DMF (c).

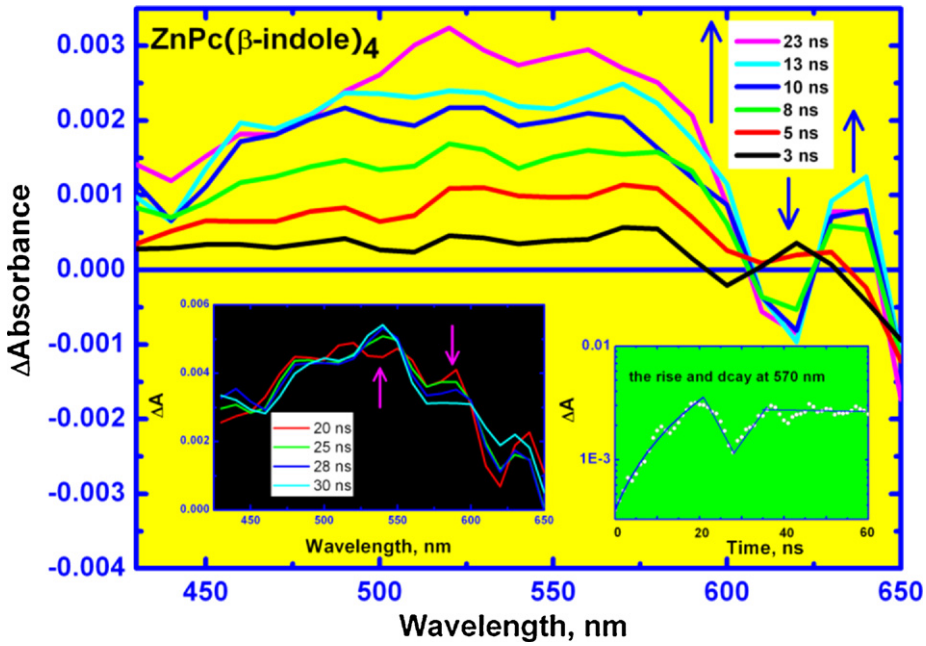

Fig. 5. ns scaled transient absorption spectra of ZnPc(β-indole)$_4$ in argon purged DMF, 15 μM, excitation wavelength 355 nm. Inset (black) shows CR of CSS to T_1 state. Inset (right) shows the absorption rise, decay and rise again at 570 nm.

positive absorption decay, indicating concomitant behavior, i.e., as the positive T_1–T_n absorption decays, the ground state is repopulated. The transient decay at 520 nm or 480 nm is also given in Fig. 4 for ZnPc(β-indole)$_4$ and ZnPc, the concomitant bleaching recovery at ground state absorption minimum is also included. These curves can all be well fit by the mono exponential function.

The triplet lifetime (τ_T) thus obtained is collected in Table 1. The τ_T values are 113 μs for ZnPc, and 107 μs for ZnPc(β-indole), respectively. The result suggests that attached indole units do not quench T_1 of ZnPc, i.e. PET or PeT from indoles to ZnPc does not occur. This is in contrast with the case of S_1 state, from which PET does proceed. The τ_T values are comparable to those of other Pcs [28,29], and are all sufficiently long for photosensitizing the production of singlet oxygen.

In air saturated DMF solution, however, the τ_T of ZnPc(β-indole)$_4$ is shortened dramatically to 0.37 μs (inset of Fig. 4c), while that of ZnPc is reduced to 0.30 μs. The rate constant by oxygen quenching can be then evaluated to be $1.35 \times 10^9\ M^{-1}\ s^{-1}$ for ZnPc(β-indole)$_4$ and $1.66 \times 10^9\ M^{-1}\ s^{-1}$ for ZnPc, which are close to diffusion rate constant. This effective oxygen quenching also suggests that the positive absorptions are indeed due to T_1–T_n triplet absorptions. The triplet absorption coefficient ($\Delta\varepsilon_T$) was determined to be 31,715 $M^{-1}\ cm^{-1}$ for ZnPc(β-indole)$_4$. The triplet formation quantum yield was measured to be 0.50, slightly smaller than 0.60 for ZnPc.

In this micro second time scale, no transient species other than T_1 was found from TAS in Fig. 4. This also shows that no triplet quenching is present, and hence no PET originates from T_1 state. Within this time range, ZnPc$^{\bullet-}$–Indole$^{\bullet+}$ due to PET from S_1 is also not observed, because the CSS is generated and decayed in nano seconds. Since two-thirds of S_1 states of ZnPc are not quenched by the conjugated indoles, ISC (intersystem crossing, i.e. process (II) below) from S_1 can still effectively proceed, which will compete with the process (III), i.e. S_1 quenching by indoles as below.

$$\text{Absorption}: \quad \text{ZnPc–indole} \xrightarrow[fs]{h\nu} \text{ZnPc}(S_1)\text{–indole} \qquad \text{(I)}$$

$$\text{ISC}: \quad \text{ZnPc}(S_1)\text{–indole} \xrightarrow[\text{ISC}]{6\,\text{ns}} \text{ZnPc}(T_1)\text{–indole} \xrightarrow{107\,\mu\text{s}} \text{ZnPc–indole} \qquad \text{(II)}$$

$$\text{PET}: \quad \text{ZnPc}(S_1)\text{–indole} \xrightarrow[\text{PET}]{6\,\text{ns}} \text{ZnPc}^{\bullet-}\text{–indole}^{\bullet+} \xrightarrow[\text{CR}]{5\,\text{ns}} \text{ZnPc–indole} \qquad \text{(III)}$$

ISC generates T_1 which is 107 μs long-lived and absorbs light in a broad range of wavelength, which may interfere with the observation of other transient species. Charge separated state (CSS), however, exhibits short lifetime of 5 ns (obtained in Section 3.3) due to easy charge recombination (CR), as shown by process (III). By recording spectra in μs scale we can therefore easily identify the transient absorptions of T_1, but not CSS since it is disappeared already.

3.3. Nano second transient absorption spectra

Fig. 5 shows the evolution of the TAS of ZnPc(β-indole)$_4$ during the first 23 ns. Absorption bands at 570 and 630 nm due to ZnPc$^{\bullet-}$ are now clearly resolvable in additional to T_1–T_n absorption band at 520 nm. The signal of ZnPc$^{\bullet-}$ rises almost at the same speed as that of T_1–T_n absorption in the first 15 s, since the rate constant of electron transfer (k_{ET}) and of triplet formation (k_{isc}) are equal (Table 1, also see process (II) and (III) above). However, the triplet signal became higher after 20 ns of excitation, due to the faster decay of CSS by CR. The formation and decay at 570 nm are illustrated in the inset of Fig. 5, which shows that CSS state has a lifetime of ca. 5 ns. The presence of ZnPc$^{\bullet-}$ absorption unambiguously indicates the presence PET from indole units to ZnPc moiety. We would then quantitatively evaluate the importance of PET relative to radiation decay (fluorescence) and ISC in the S_1 decay of ZnPc moiety. In air saturated DMF solutions, the absorption bands at 570 and 630 nm were quenched, indicating molecular oxygen can effectively react with ZnPc$^{\bullet-}$ by capturing the electron: $\text{ZnPc}^{-} + O_2 \rightarrow \text{ZnPc} + O_2^{\bullet-}$. The formed $O_2^{\bullet-}$ can be trapped by DMPO and recorded by ESR, for which we have reported previously [30].

3.4. Fluorescence studies

The fluorescence emission spectra of ZnPc(β-indole)$_4$ in DMF were recorded under the same condition as that of ZnPc with excitation at 610 nm. These spectra are compared in Fig. 6. In addition to the intensity quenching mentioned previously, the spectral shape

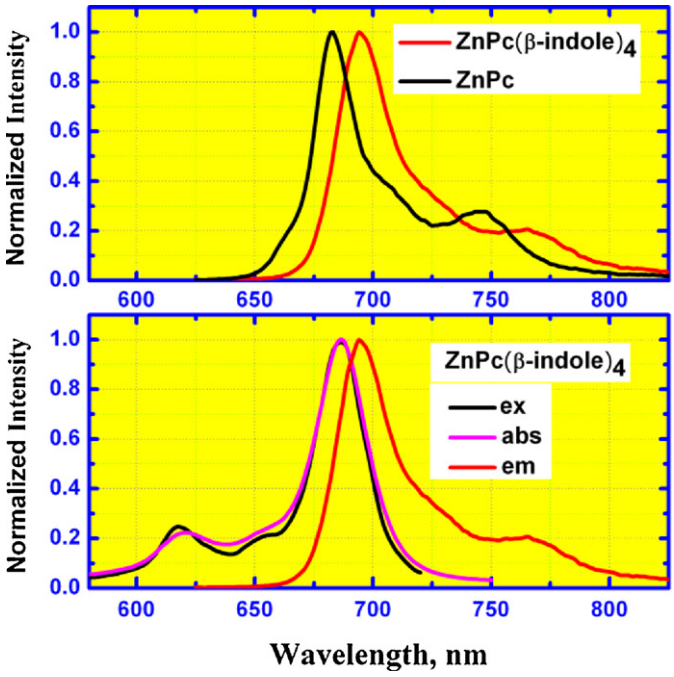

Fig. 6. (Top) Normalized fluorescence emission spectra with excitation at 610 nm (absorbance 0.090), (bottom) normalized absorption, fluorescence excitation (emission at 730 nm) and emission spectra (with excitation at 610 nm) for ZnPc(β-indole)$_4$.

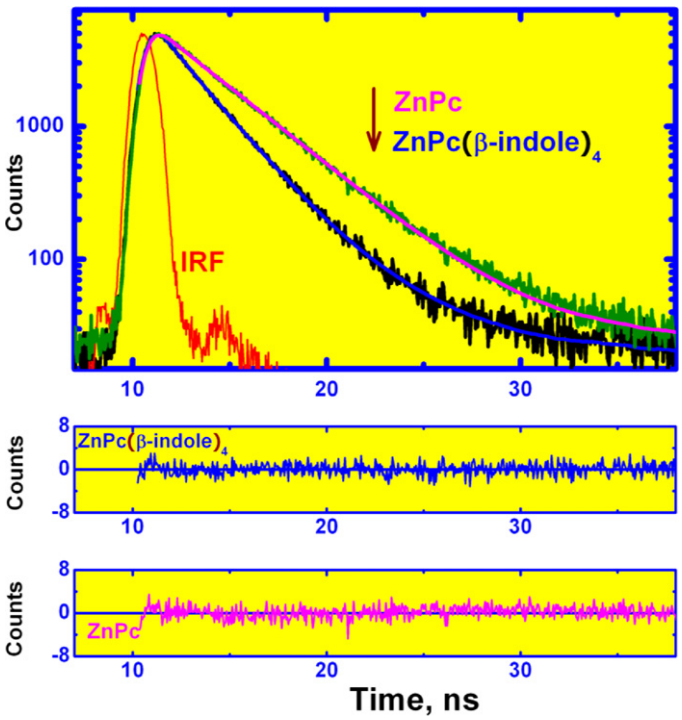

Fig. 7. (Top) time profile of fluorescence decay of with excitation at 672 nm diode laser (50 *ps*), the emission was monitored at 690 nm, the concentration of dyes is ca. 2.0 μM. Middle and bottom: fitting residues.

also becomes broader, the width of half height is increased from 24.5 nm of ZnPc to 29.5 nm of ZnPc(β-indole)$_4$. The spectral shape in the region above 720 nm also shows difference. The band broadening and the shape change indicate the presence of a new minor emission band. Φ_f of ZnPc(β-indole)$_4$ is 0.20, decreased from 0.30 of ZnPc. This fluorescence quenching is reasonable, because indole units contain a nitrogen atom and can act as electron donors for PET, so do tryptophan residues in peptides or proteins.

The transient decay of fluorescence emission at 690 nm is illustrated in Fig. 7. A visual examination already tells that the fluorescence lifetime (τ_f) of ZnPc(β-indole)$_4$ is shortened with respect to that of ZnPc. While ZnPc exhibits a typical mono-exponential decay with τ_f of 3.60 ns, ZnPc(β-indole)$_4$ shows bi-exponential decaying behavior, suggesting the presence of two emitting species, matching the observation from emission spectrum. The short-lived component has a τ_f of 2.22 ns and is responsible for 87% emission while the long one has a τ_f of 4.91 ns and takes the possession of 13% emission. The τ_f of major emitting species is significantly shortened to 61.6% of the value for free ZnPc, apparently due to PET from indole moieties to the excited singlet state (S_1) of ZnPc sub-unit in the conjugate. The de-excitation of S_1 is often bi-exponential when PET is involved in the process. Two emitting species are usually responsible for the bi-exponential behavior: (i) CSS emission due to CR (charge recombination process (IV)), and (ii) part of D–A (S_1) with the unfavourable conformation for PET.

$$\text{CR fluorescence}: \quad \text{ZnPc}^{\bullet-}\text{–indole}^{\bullet+} \xrightarrow[\text{CR}]{5\text{ ns}} \text{ZnPc–indole} + h\nu \qquad \text{(IV)}$$

For CR fluorescence, a red-shifted, weak and broader emission usually occurs due to the lower energy level of $D^{\bullet+}$–$A^{\bullet-}$ than D–A(S_1). For D–A(S_1) with the unfavourable conformation, the τ_f of minor component is close to that for free ZnPc due to the absence of PET, and no new emission band is expected in this case. In this particular case, the minor component is due to CSS emission since its lifetime is 4.91 ns, quite longer than 3.60 ns of free ZnPc. The broader emission spectrum also implicates the contribution from other emitting species. Monitoring the decay at 730 nm, a bi-exponential fitting is also necessary but the percentage of long-lived component is increased to 39% from 13% at 690 nm, since emission maximum of CSS is located in this region.

In summary, the fluorescence investigation reveals that PET does occur from indole units to ZnPc fragment within the conjugate. With excitation at 610 nm, only ZnPc moiety is populated to S_1, energy transfer from S_1 of ZnPc to indole is not allowed, since the emitted photons have much lower energy than that of indoles can absorb. CSS charge recombination also emits fluorescence with the lifetime of 4.91 ns. This τ_f value is actually the lifetime of CSS itself, which is in good agreement with the value of 5.0 ns obtained from the decay of transient absorption of $ZnPc^{\bullet-}$ at 570 nm.

3.5. *Efficiency and kinetics of PET*

The rate constant of PET (k_{et}) can be calculated from the fluorescence lifetime data using Eq. (5), in which τ_f^0 is the fluorescence lifetime of ZnPc while τ_f is the value of short-lived component for ZnPc(β-indole)$_4$. k_{et} is thus obtained as $0.17 \times 10^9\ s^{-1}$.

$$k_{et} = \tau_f^{-1} - (\tau_f^0)^{-1} \qquad (5)$$

Efficiency for PET (Φ_{et}) is calculated to be 38% by using the k_{et} value ($\Phi_{et} = k_{et}\tau_f$), which indicates that PET efficiency is almost double of its fluorescence emission ($\Phi_f = 0.20$) in the system. k_f (the rate constant of fluorescence emission from S_1) is $0.90 \times 10^8\ s^{-1}$ and $0.83 \times 10^8\ s^{-1}$ for ZnPc(β-indole)$_4$ and ZnPc, respectively (computed by $k_f = \Phi_f/\tau_f$), showing no remarkable change.

The summation of Φ_f, Φ_{et}, and Φ_T is 1.08 (=0.20 + 0.38 + 0.5) for ZnPc(β-indole)$_4$, larger than 0.90 (=$\Phi_f + \Phi_T$ = 0.30 + 0.60) for ZnPc. The internal conversion (IC) efficiency of ZnPc can be estimated as 0.10 ($\Phi_{ic} = 1 - \Phi_f - \Phi_T$). The substitution of H by indole is expected to enhance IC, such that Φ_{ic} of ZnPc(β-indole)$_4$ is likely greater than 0.10. Therefore the summation of Φ_f, Φ_{et}, Φ_{ic} and Φ_T for ZnPc(β-indole)$_4$ would be larger than 1.18. This large value caused our attention. While the repeated measurements for Φ_f, Φ_{et} and

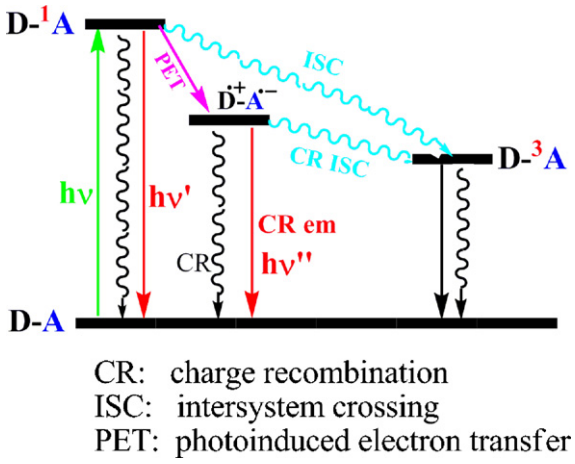

Fig. 8. The formation of CSS ($D^{\bullet+}$–$A^{\bullet-}$) by PET, and CR of CSS to generate T_1 and emission.

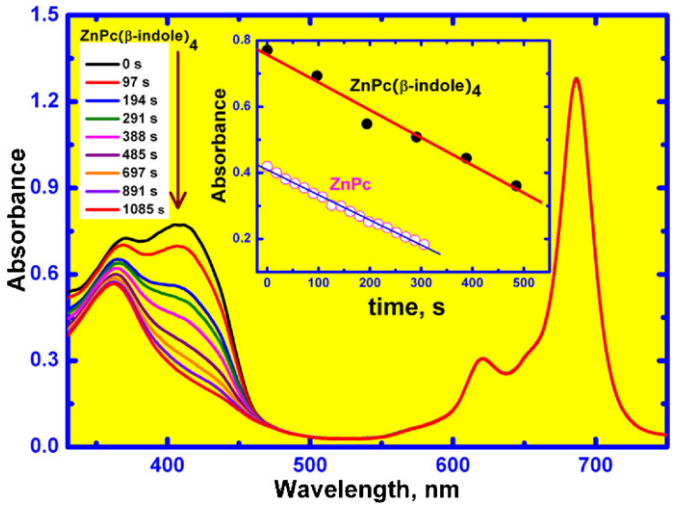

Fig. 9. The change of absorption spectrum of upon irradiation time in air saturated DMF containing 5 μM DPBF and 11 μM photosensitizer with irradiation at 660 nm. Inset is the linear plot of absorbance at 415 nm against irradiation time.

Φ_T showed reproducible values, we noticed Φ_T is larger than that anticipated, because CR of CSS also generate T_1 state. Fig. 8 gives the TAS during 20–40 ns. With the decrease of the band for $ZnPc^{\bullet-}$ at 570 nm, the T_1–T_n absorption is concurrently increased, indicating that CR of CSS also forms triplet state T_1 of ZnPc:

$$\text{CR to } T_1: \quad ZnPc^{\bullet-}\text{–indole}^{\bullet+} \xrightarrow{CR-ISC} ZnPc(T_1)\text{–indole} \qquad (V)$$

The absorption change at 570 nm (where both $ZnPc^{\bullet-}$ and T_1 absorb) with time, inset of Fig. 5, shows all the processes: (1) first rise stage: both $ZnPc^{\bullet-}$ and T_1 are formed after laser excitation, (2) fast decay of $ZnPc^{\bullet-}$ due to CR of $ZnPc^{\bullet-}$–$Indole^{\bullet+}$, (3) CR of CSS to form T_1, (4) T_1 decay. These processes are illustrated in Fig. 8. The presence of CR-ISC is the reason why the observed Φ_T (0.50) is bigger than the expected value of 0.32, which is only due to ISC from S_1 ($1-\Phi_f-\Phi_{et}-\Phi_{ic} \le 1-0.2-0.38-0.1=0.32$). This means that almost half of CSS ($(0.50-0.32)/0.38=47\%$) goes to triplet state, i.e. process (V) plays an important role in CR of CSS.

3.6. Thermodynamics of PET

The oxidation potential of methyl-indole was measured to be 0.65 V [31], while the reduction potential of the phthalocyanine ring is −0.90 V in DMF [32]. The electron transfer from indole to ZnPc ring in their ground states is not thermodynamically allowed, due to the large positive value of free energy change (ΔG) calculated by $\Delta G_{ET}=E_{ox}-E_{red}-C=0.65-(-0.85)-0.06=1.44$ eV, in which E_{ox} is the oxidation potential of a donor, E_{red} represents the reduction potential of an acceptor, and C is a small constant associated with solvent. PET from indole to S_1 of ZnPc moiety (by the photo excitation of the Pc moiety), on the other hand, is thermodynamically favored, since its ΔG is a negative value obtained by: $\Delta G_{PET}=\Delta G_{ET}-E_{00}$ (ZnPc) = 1.44 − 1.83 = −0.39 eV. PET from indole donors to T_1 of ZnPc moiety is forbidden, since the energy of the T_1 state is 0.99 eV, which suggests a ΔG of +0.45 eV.

3.7. Singlet oxygen formation and DPBF photooxidation

The quantum yield (Φ_Δ) for photooxidation was measured using the DPBF chemical trapping method with irradiation at 660 nm in air saturated DMF. DPBF degradation was monitored by UV–vis spectra. Fig. 9 displays the decrease of [DPBF] upon irradiation time, for which the first order kinetics was observed (inset of Fig. 9). Φ_Δ is also included in Table 1. The measured value of Φ_Δ for ZnPc(β-indole)$_4$ is 0.72, while the maximum quantum yield of singlet oxygen $^1O_2$ ($^1\Delta_g$) production is expected to be the value of Φ_T, i.e. 0.50, since it is generated by energy transfer from T_1 state to molecular oxygen:

$$T_1(PS)+{}^3O_2 \rightarrow S_0(PS)+{}^1O_2({}^1\Delta_g) \qquad (VI)$$

$$DPBF+{}^1O_2({}^1\Delta_g) \rightarrow \text{producttypeII} \qquad (VII)$$

The measured Φ_Δ of 0.72 is significantly greater than the maximum quantum yield of singlet oxygen (0.50). This is due to the fact that DPBF traps not only singlet oxygen but also superoxide anion radical $O_2^{\bullet-}$[33]. Therefore the measured photooxidation efficiency is the sum of two types of oxidations: (1) DPBF oxidized by singlet oxygen, and (2) DPBF oxidized by superoxide anion radical $O_2^{\bullet-}$.

For the conjugate, superoxide anion radical $O_2^{\bullet-}$ is produced by the reaction of $ZnPc^{\bullet-}$ with molecular oxygen (process (VIII) below), this is evidenced by the oxygen quenching to TA of $ZnPc^{\bullet-}$ at 570 nm mentioned previously. In contrast, free ZnPc has no this process.

$$ZnPc^{\bullet-}\text{–}Indole^{\bullet+}+O_2 \rightarrow ZnPc\text{–}Indole^{\bullet+}+O_2^{\bullet-} \qquad (VIII)$$

$$DPBF+O_2^{\bullet-} \rightarrow \text{producttypeI} \qquad (IX)$$

The quantum efficiency for CSS generation is 0.38 (Φ_{ET}). In the presence of oxygen process (V), i.e. CR to T_1, is inhibited, such that all CSS is dissipated in process (VIII), which gives the maximum quantum efficiency of $O_2^{\bullet-}$ generation as 0.38. In this case, all T_1 is originated from S_1 by ISC, the efficiency of which is 0.32, this is the amount of T_1 that can contribute to the generation of singlet oxygen. Therefore the total efficiency of DPBF photooxidation is expected to be the sum of process (VII), i.e. Type II reaction, and process (IX), i.e. Type I reaction. The summation gave the value 0.70 (=0.38 + 0.32). This estimated value is in good agreement with the measured value of 0.72.

We can also roughly estimate the relative importance of Type I over Type II reaction. The percentage of Type I reaction is about 54% (0.38/0.70), while the importance of Type II reaction is 46%. This result shows that the binding of indole can affect the reaction mechanism significantly, while the photo-oxidizing ability of the bioconjugated PS is even increased.

4. Conclusion

We have synthesized a bioconjugated PS (BCPS) model compound in which four indole units were attached to ZnPc through

covalent bonding. The photophysical and photochemical processes related to PDT were revealed by comparing the transient and steady state spectra of S_1, T_1 and CSS with that of the free ZnPc. PET occurs within the molecule from indole subunits to S_1 of ZnPc moiety, which is evidenced by the quenching of Φ_f and τ_f, the presence of transient absorption bands for $ZnPc^{\bullet-}$, the emission due to CSS, the thermodynamic and kinetic analysis. The indole conjugated ZnPc shows unusually high yield for triplet formation because CR of CSS ($ZnPc^{\bullet-}$–$indole^{\bullet+}$) is recombined to triplet state ZnPc(T_1)–indole. The yield for DPBF photooxidation is higher than that of ZnPc, due to the good yield of superoxide anion radical generated by the reaction of CSS with oxygen (which is absent for free ZnPc). Type I mechanism accounts for 54% of total reaction, which is higher than 46% by Type II reaction. These results suggest that the indole-modified ZnPc is a better PS than the free ZnPc, but the reaction mechanism is altered so that the importance of Type I mechanism is significantly enhanced.

Acknowledgements

This work has been supported by Hebei Provincial Science Foundation (Contract B2010001518) and HBUST.

References

[1] C.A. Robertson, D.H. Evans, H. Abrahamse, J. Photochem. Photobiol. B 96 (2009) 1–8.
[2] N.V. Kudinova, T.T. Berezov, Biochem. (Moscow) Suppl. Ser. B: Biomed. Chem. 4 (2010) 95–103.
[3] K. Plaetzer, B. Krammer, J. Berlanda, F. Berr, T. Kiesslich, Lasers Med. Sci. 24 (2009) 259–268.
[4] J.J. Lopez, M.A.G. Carter, Y.P. Tsentalovich, O.B. Morozova, A.V. Yurkovskaya, P.J. Hore, Photochem. Photobiol. 75 (2002) 6–10.
[5] X.-F. Zhang, H. Xu, T. Shen, Sci. China B 38 (1995) 641–648.
[6] G. Ferraudi, G.A. Arguello, H. Ali, J.E. Lier, Photochem. Photobiol. 47 (1988) 657–660.
[7] X.F. Zhang, H.J. Xu, J. Photochem. Photobiol. B 24 (1994) 109–116.
[8] A. Segalla, C.D. Borsarelli, S.E. Braslavsky, J.D. Spikes, G. Roncucci, D. Dei, G. Chiti, G. Jori, E. Reddi, Photochem. Photobiol. Sci 1 (2002) 641–648.
[9] J. Davila, A. Harriman, Photochem. Photobiol. 50 (1989) 29–35.
[10] W.M. Sharman, J.E. Lier v, Bioconjugate Chem. 16 (2005) 1166–1175.
[11] G. Valduga, S. Nonell, E. Reddi, G. Jori, S.E. Braslavsky, Photochem. Photobiol. 48 (1988) 1–5.
[12] R.M. Negri, A. Zalts, E.A. RomáN, P.F. AramendíA, S.E. Braslavsky, Photochem. Photobiol. 53 (1991) 317–322.
[13] N. Cauchon, H. Tian, R. Langlois, C. La Madeleine, S. Martin, H. Ali, D. Hunting, J.E. van Lier, Bioconjugate Chem. 16 (2005) 80–89.
[14] X.F. Zhang, H.J. Xu, J. Chem. Soc., Faraday Trans. 89 (1993) 3347–3351.
[15] C.F. Choi, P.T. Tsang, J.D. Huang, E.Y.M. Chan, W.H. Ko, W.P. Fong, D.K.P. Ng, Chem. Commun. 2004 (2004) 2236–2237.
[16] T. Nyokong, Coord. Chem. Rev. 251 (2007) 1707–1722.
[17] S.-i. Ogura, K. Tabata, K. Fukushima, T. Kamachi, I. Okura, J. Porphyrins Phthalocyanines 10 (2006) 1116–1124.
[18] D. Woehrle, O. Suvorovab, R. Gerdesa, O. Bartelsa, L. Lapoka, N. Baziakinab, S. Makarovb, A. Slodeka, J. Porphyrins Phthalocyanines 8 (2004) 1020–1041.
[19] V. Mantareva, V. Kussovski, I. Angelov, E. Borisova, L. Avramov, G. Schnurpfeil, D. Woehrle, Bioorg. Med. Chem. 15 (2007) 4829–4835.
[20] N. Yusuf, S.K. Katiyar, C.A. Elmets, Photochem. Photobiol. 84 (2008) 366–370.
[21] J.D. Miller, E.D. Baron, H. Scull, A. Hsia, J.C. Berlin, T. McCormick, V. Colussi, M.E. Kenney, K.D. Cooper, Toxicol. Appl. Pharmacol. 224 (2007) 290–299.
[22] M. Montalti, A. Credi, L. Prodi, M.T. Gandolfi, Photophysical properties of organic compounds, in: Handbook of Photochemistry, Taylor & Francis Group, LLC, London, 2006, 255.
[23] K. Ishii, N. Kobayashi, The photophysical properties of phthalocyanines and related compounds, in: K.M. Kadish, K.M. Smith, R. Guilard (Eds.), The Porphyrin Handbook, vol. 16, Academic Press, New York, Amsterdam, 2003, pp. 1–42.
[24] I. Carmichael, G.L. Hug, J. Phys. Chem. Ref. Data 15 (1986) 1–250.
[25] M.G. Lagorio, L.E. Dicelio, E.A.S. Roman, S.E. Braslavsky, J. Photochem. Photobiol. B 3 (1989) 615–624.
[26] N. Kuznetsova, N. Gretsova, E. Kalmykova, E. Makarova, S. Dashkevich, V. Negrimovskii, O. Kaliya, E. Luk'yanets, Russ. J. Gen. Chem. 70 (2000) 133–139.
[27] N.B. McKeown, The synthesis of symmetrical phthalocyanines, in: K.M. Kadish, K.M. Smith, R. Guilard (Eds.), The Porphyrin Handbook, vol. 15, Academic Press, New York, 2003, p. 61.
[28] X.-F. Zhang, Y. Chang, Y. Peng, F. Zhang, Aust. J. Chem. 62 (2009) 434–440.
[29] X.F. Zhang, J. Huang, H. Zhao, X. Zheng, Z. Junzhong, J. Photochem. Photobiol. A: Chem. 215 (2010) 96–102.
[30] X.F. Zhang, H.J. Xu, D.W. Chen, J. Photochem. Photobiol. B: Biol. 22 (1994) 235–239.
[31] Y.A. Udum, M. Düdükcüa, F. Kölelia, React. Funct. Polym. 68 (2008) 861–867.
[32] M. L'her, A. Pondaven, Electrochemistry of Phthalocyanines, in: K.M.S.K.M. Kadish, R. Guilard (Eds.), The Porphyrin Handbook, Academic Press, San Diego, 2003, pp. 117–170.
[33] T. Ohyashiki, M. Nunomura, T. Katoh, Biochim. Biophys. Acta (BBA): Biomem. 1421 (1999) 131–139.